Acta Cryst. (1985). A41, 223-227

Characterization of Process-Induced Defects in Silicon with Triple-Crystal Diffractometry

A. A. LOMOV

A. V. Shubnikov Institute of Crystallography of the Academy of Sciences of the USSR, Leninsky prospect 59, Moscow 117333, USSR

AND P. ZAUMSEIL AND U. WINTER

Institut für Physik der Werkstoffbearbeitung der Akademie der Wissenschaften der DDR, 1166 Berlin-Rahnsdorf, Seestrasse 82, German Democratic Republic

(*Received* 26 *March* 1984; *accepted* 1 *November* 1984)

Abstract

With a triple-crystal diffractometer of parallel $(n, -n, n)$ setting, X-ray diffuse scattering has been observed from a silicon crystal containing process-induced defects. It is shown that the use of a conventional X-ray tube with 1.5 kW power guarantees the registration of defects with characteristic size $R \simeq 1{\cdot}8$ μm and concentration $C_0 \simeq 1 \times 10^9$ cm^{-3}. The theoretical simulations of the diffuse scattering were carried out based on the Huang theory. The data of TEM investigations show stacking faults of interstitial type with radius $R_L \simeq 0{\cdot}9$ μm and concentration $C_L \simeq 2 \times 10^9$ cm^{-3}, as well as small precipitates, in the specimen.

1. Introduction

X-ray diffuse scattering has been used as a powerful method for studying lattice defects in recent years. It has found a wide field of application, especially investigating point defects and their clusters or small loops after irradiation of different materials (Spalt, 1970; Lohstöter, Spalt & Peisel, 1972; Larson & Young, 1973; Ehrhard & Schilling, 1974; Lal, 1981; Mayer & Peisel, 1982). In most of these cases simple diffractometer arrangements with a curved monochromator crystal are used because the defects are very small and the angular region of Huang scattering is large enough so that the resolution limit by slit systems is acceptable.

Increasing defect size leads to a restriction of the Huang scattering to the immediate vicinity of the Bragg peak. In this case it is necessary to use a double-crystal diffractometer or better a triple-crystal diffractometer in parallel position to increase the resolution and to measure the distribution of diffuse scattering in an integral (Thomas, Baldwin & Dederichs, 1971; Patel, 1975) or in differential geometry (Larson & Schmatz, 1974; Iida & Kohra, 1979; Iida, 1979; Zaumseil & Winter, 1982*b*), respectively.

The aim of the present work is to demonstrate that a complete characterization of relatively large defects is possible by the measurement of diffuse scattering with a triple-crystal diffractometer of parallel $(n, -n, n)$ setting. This is shown for process-induced defects in silicon. Experimental results from X-ray scattering are compared with theoretical simulations and with TEM investigations.

2. Experimental

X-ray measurements of the (111) Bragg reflection with different wavelengths (Mo $K\alpha$, Cu $K\alpha$, Co $K\alpha$, Cr $K\alpha$) were carried out with a triple-crystal diffractometer (TCD) of parallel $(n, -n, n)$ setting as shown in Fig. 1. A conventional X-ray tube with 1·5 kW power and apparent focal size 0·5 × 1·0 mm was used. Two different kinds of measurements were realized, namely, measurements on the Ewald sphere at a fixed position α of the sample with $\Delta\theta$ rotation of the analyzer crystal to obtain information on both dynamical and kinematical diffraction, and measurements at position $\Delta\theta = 0$ with α rotation of the sample to investigate the decrease of diffuse scattering *versus* the distance from the reciprocal-lattice point, *i.e.* in the direction perpendicular to the reciprocal-lattice vector, where the influence of the perfect lattice is minimized.

The sample was a (111) Czochralski-grown silicon wafer with a thickness of 350 μm and initial oxygen content of 9×10^{17} cm^{-3}. It was heat treated by multistep annealing. Such treatment of a silicon wafer is

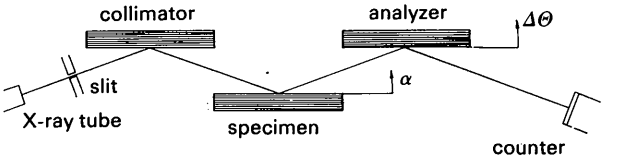

Fig. 1. Principal scheme of the triple-crystal diffractometer arrangement.

0108-7673/85/030223-05$01.50

© 1985 International Union of Crystallography

necessary for VLSI fabrication (intrinsic gettering) to produce a defect-denuded zone on the surface near the device and to create oxygen precipitates with secondary defects in the bulk of the wafer (Richter, Mai, Kirscht, Gaworzewski, 1983). A surface layer 30 μm thick was removed by etching to avoid the influence of a defect-denuded zone. Thus, only the defects of the bulk material were investigated.

3. Results

Fig. 2 shows a set of TCD intensity curves measured with different wavelengths at $\alpha = 50''$. At $\Delta\theta \simeq 0''$ a strong peak of diffuse scattering can be observed that is generated by defects in the crystal. Pseudo peak and main peak are found at $\Delta\theta = 50''$ and $\Delta\theta = 100''$, respectively. With increasing wavelengths the intensity of the diffuse scattering decreases with respect to the dynamical pseudo and main peaks.

At higher values of α the peak of diffuse scattering splits into two maxima of different heights as can be seen in Fig. 3. The maximum intensity at positive values of $\Delta\theta$ is higher than that at negative $\Delta\theta$. Measurements at negative α positions show the reverse behavior.

To obtain the distribution of diffuse scattering around the reciprocal-lattice point, a set of TCD intensity curves was analyzed. The relation between the angle positions α and $\Delta\theta$ and the scattering vector $\mathbf{q} = (q_x, q_y)$ is given by

$$(q_x, q_y) = [\Delta\theta \cos\theta_B, (2\alpha - \Delta\theta)\sin\theta_B]/\lambda. \quad (1)$$

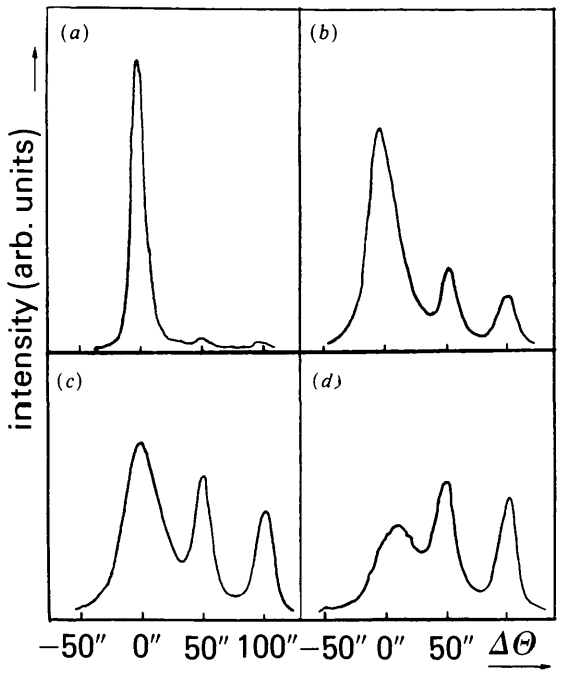

Fig. 2. TCD intensity curves of (111) reflection measured at $\alpha = 50''$ with different wavelengths. (*a*) Mo $K\alpha$, (*b*) Cu $K\alpha$, (*c*) Co $K\alpha$, (*d*) Cr $K\alpha$.

Fig. 4 shows the two-dimensional plot of equi-intensity curves in the plane of reflection measured with Co $K\alpha$ radiation. These contours are mainly caused by the scattering of lattice defects. Dynamical effects of perfect-crystal parts are only indicated by two so-called pseudo streaks (which are inclined to the q_x axis at the Bragg angle $\theta_B = 16{\cdot}6°$) and by the so-called main streak exactly directed along q_x (Iida & Kohra, 1979; Zaumseil & Winter, 1982*a*).

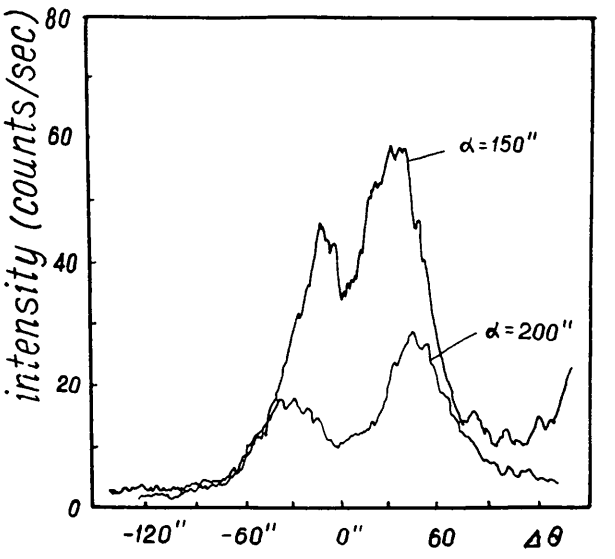

Fig. 3. TCD intensity curves of the diffuse scattering measured with Co $K\alpha$ radiation, (111) reflection, at $\alpha = 150''$ and $\alpha = 200''$.

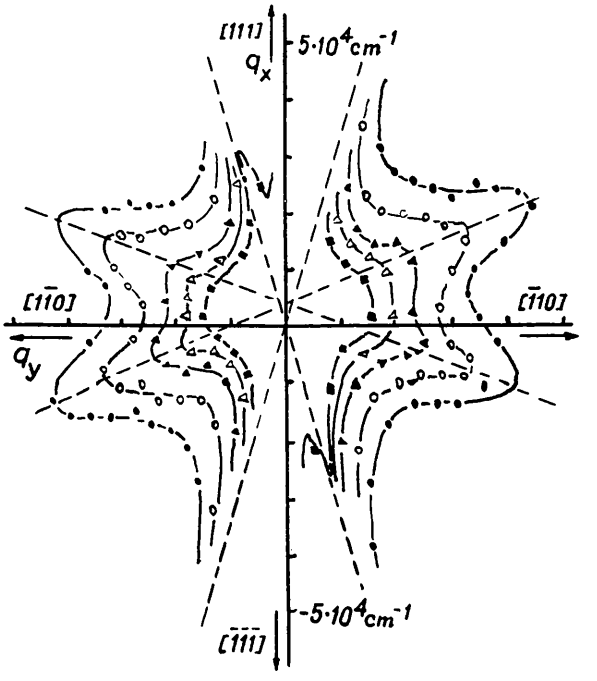

Fig. 4. Equi-intensity contours near the 111 reciprocal-lattice point, Co $K\alpha$ radiation.

Apart from these dynamical effects the contours of diffuse scattering show two directions of increased intensity, and they seem to be shifted in the [111] direction.

Measurements of diffuse scattering in the [1$\bar{1}$0] direction are shown in Fig. 5. The double-logarithmic plots of normalized intensity *versus* α position or q_x indicate two different regions with slope $s=-2$ and $s=-4$, respectively. For all wavelengths the change between the two regions occurs near $\log \alpha' \simeq 1{\cdot}5$ and $\log q'_y \simeq 3{\cdot}7$, respectively, where α is measured in seconds of arc and q_y in cm^{-1}.

4. Discussion

Characterization of defects means that information can be obtained about their concentration, size, shape and type. The basis of the following theoretical description and comparison with experimental results is the formalism of Dederichs (1971, 1973). The scattering power is given by

$$I(\mathbf{h}+\mathbf{q}) = I_0 \frac{(r_0 F)^2}{2\mu} \int_{-\infty}^{\infty} S(\mathbf{h}+\mathbf{q})\, \mathrm{d}\Omega, \qquad (2)$$

where I_0 is the incident X-ray intensity, μ is the linear absorption coefficient, $r_0 F$ is the product of the classical electron radius, r_0, and the atomic scattering factor, F, including thermal and polarization effects. The distribution of diffuse scattering is described by the scattering function $S(\mathbf{h}+\mathbf{q})$ and the integration takes place over the solid angle of the detector. In the case of the chosen diffractometer with the parallel triple-crystal arrangements the horizontal divergency is limited by the half-width of the reflection curve of the analyzer crystal, being small compared with the angular distribution of diffuse scattering. Thus, only the vertical divergency restricted by a slit system must be considered in the integration. The vertical angular resolution corresponds to an order of 10^5 cm^{-1} in the reciprocal space.

The symmetrical part of Huang scattering occurring in the region with $q \ll 1/R_0$, where R_0 is a characteristic defect radius, is given by (Dederichs, 1971, 1973)

$$S^s(\mathbf{h}+\mathbf{q}) = \frac{C_d}{V_c^2} |\mathbf{h} \cdot \mathbf{t}(\mathbf{q})|^2, \qquad (3)$$

where C_d is the defect concentration, V_c is the volume of the unit cell, and $\mathbf{t}(\mathbf{q})$ represents the Fourier transform of the asymptotic displacement field of the defects. In the case of the existence of different defects, the scattering function will be obtained as the sum over the scattering functions of the individual kinds of defects (Dederichs, 1971, 1973). This relation between the scattering curves in the reciprocal space and the displacement field of the defects allows, in principle, the defect shape and orientation to be determined.

Fig. 6 shows calculated intensity contours of dislocation loop arrangements with [111], [110] and [100] orientation and of isotropic defects in the (11$\bar{2}$) plane, and the plane of reflection. The calculations are based on the formalism of Dederichs (1971, 1973) including the anisotropy of the silicon crystal. The simulations of TCD intensity curves of the same defect arrangements as shown in Fig. 6 are given in Fig. 7 at $\alpha = 150''$. They are calculated for the conditions of a TCD arrangement with Co $K\alpha$-(111) reflection with the loop radius $R_L = 1$ μm, loop concentration $C_L = 1\times10^9$ cm^{-3}, Burgers vector $|b| = 1{\cdot}05$ Å and with vertical resolution $\Omega_v = 1\times10^5$ cm^{-1}. The comparison of the theoretical results in Figs. 7 and 6 with Figs. 3

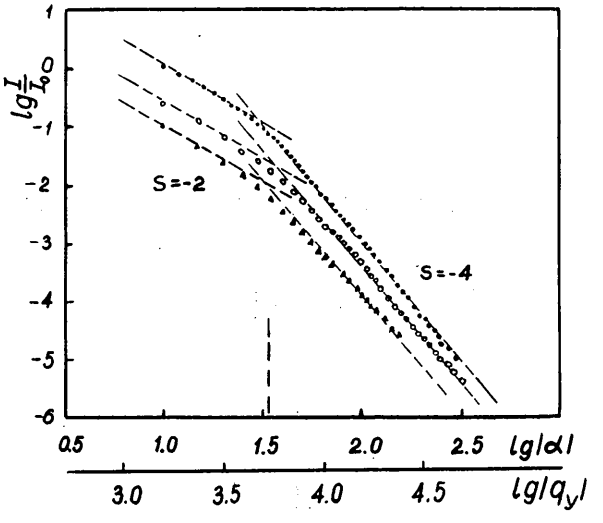

Fig. 5. Double-logarithmic plot of normalized intensity *versus* α position measured at $\Delta\theta = 0''$ ([1$\bar{1}$0] direction) with different radiations: ● Mo $K\alpha$; ○ Co $K\alpha$; △ Cr $K\alpha$.

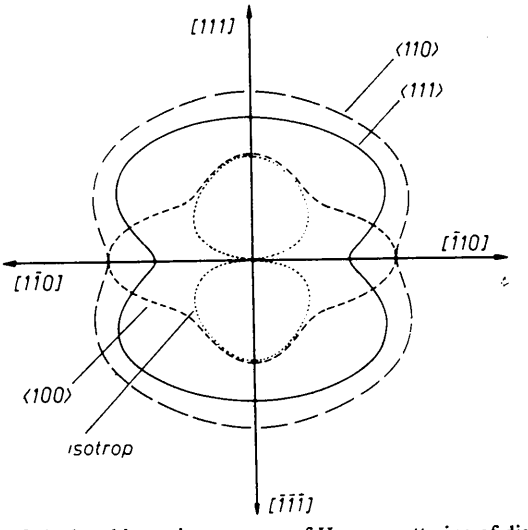

Fig. 6. Calculated intensity contours of Huang scattering of dislocation loop arrangements with [111], [110] and [100] orientation and of isotropic defects.

and 4 indicates that the best agreement between experimental and theoretical curves can be achieved with the arrangement of [111]-oriented stacking faults, although the experimental curves are more strongly shaped than the theoretical ones.

An asymmetry of diffuse scattering as would be expected from the antisymmetric part of Huang scattering (Dederichs, 1971; Larson & Barhorst, 1981) is not observed as shown in Fig. 4. Nevertheless, the shift of the equi-intensity contours can be explained by the lattice contraction around defects with a positive misfit volume (interstitial type).

In the region of Huang scattering ($q \ll 1/R_0$) the scattering power is proportional to $1/q^2$, whereas for $q > 1/R_0$ it decreases more rapidly, proportional to $1/q^4$. This situation is well demonstrated in Fig. 5. Moreover, it must be emphasized that the curves in Fig. 5 are obtained by correcting the experimental results to take account of the bad vertical resolution. Therefore, normalized intensities greater than unity can be obtained theoretically.

The transition from $1/q^2$ to $1/q^4$ scattering law allows a rough estimation of the defect size. From $R \simeq 1/q'_y$ follows the characteristic defect radius $R_0 \simeq 1{\cdot}8\ \mu$m. From (2) and (3) with

$$\mathbf{h} \,.\, \mathbf{t}(\mathbf{q}) = (b\pi R_L^2 h/q)\, K(\mathbf{h}, \mathbf{b}, \mathbf{q}) \qquad (4)$$

for circular loops with radius R_L and Burgers vector $\mathbf{b}$, the defect concentration can be estimated. $K(\mathbf{h}, \mathbf{b}, \mathbf{q})$ describes the angular distribution of diffuse scattering and is of the order of unity (Dederichs, 1971). Owing to the R_L^4 dependence of the scattering intensity, the accuracy of the defect concentration strongly depends on the accuracy of the determination of the loop radius (Larson, 1975).

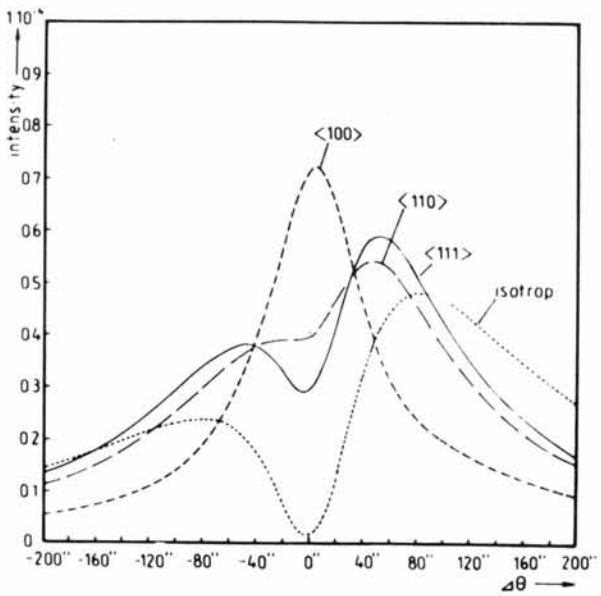

Fig. 7. Calculated TCD intensity curves at $\alpha = 150''$ of the same defects as in Fig. 6.

TEM investigations were carried out to prove the results obtained and to obtain exact information about the relation between the calculated characteristic defect (loop) radius and the real defect radius. Fig. 8 shows a transmission electron micrograph of the specimen investigated. It confirms the result of X-ray investigations. The large defects are stacking faults of interstitial type on {111} planes. The average loop radius amounts to $R_L \simeq 0{\cdot}9\ \mu$m and the loop concentration is $C_L \simeq 2 \times 10^9\ \text{cm}^{-3}$. Besides these loops much smaller precipitates are observed. Since the diffuse scattering very strongly depends on the defect size and, on the other hand, the concentration of the precipitates is only five times higher than that of the loops, it can be concluded that the observed diffuse scattering is nearly completely caused by the large loops.

As a result of the comparison between the calculated defect radius of X-ray measurements and the observed loop radius by TEM it follows that $R_L \simeq \frac{1}{2}R_0$. Using this relation and the intensity of diffuse scattering in the region of $1/q^2$ dependence in Fig. 5, a loop concentration of $C_L \simeq 1 \times 10^9\ \text{cm}^{-3}$ can be estimated for Co and Cr radiation and $C_L \simeq 0{\cdot}4 \times 10^9\ \text{cm}^{-3}$ for Mo radiation. This smaller value can be explained by the small thickness of the specimen, so that the assumption about an infinitely thick crystal was not fulfilled in the Mo case. These results show, in spite of the difference of the two methods, a rather good agreement.

The differences between the shapes of experimental and theoretical curves of (111) loop arrangements (Figs. 4, 6 and 3, 7) can be explained as follows.

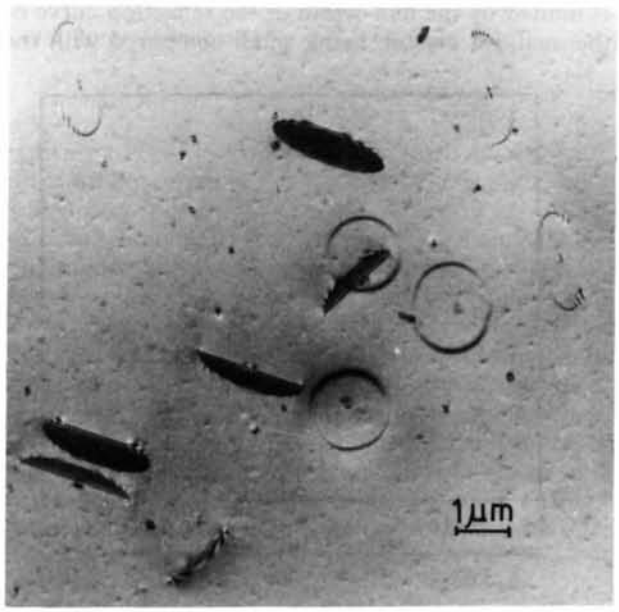

Fig. 8. Transmission electron micrograph of the specimen investigated showing [111] stacking faults and precipitates.

On the one hand, the greatest part of the equi-intensity curves in Fig. 4 and the TCD curves in Fig. 3 are measured in regions with $q > 1/R_0$. Here (3), which the calculations are based on, is never valid, and the angular distribution of diffuse scattering should be changed. On the other hand, since the defects are very large, surface relaxation of the displacement fields and dynamical effects of X-ray diffraction will be of importance. One disadvantage of this method is the domination of the diffuse scattering caused by the larger defects in the case of a mixture of defects of different size. In the case described the small precipitates, observed by TEM, were not detectable by X-ray measurements.

Nevertheless, the results presented show that it is possible to characterize defects even up to 1 μm in size by the non-destructive method of X-ray diffuse scattering with TCD and by calculations based on the simple theory of Huang scattering.

The authors wish to thank E. Bugiel for the TEM results obtained at the HVEM of the IFE Halle and Dr C. Becker, Dr R. M. Imamov and Dr A. A. Zavyalova for their interest in the work, helpful discussions and for carefully reading the manuscript.

References

DEDERICHS, P. H. (1971). *Phys. Rev. B*, **4**, 1041-1050.

DEDERICHS, P. H. (1973). *J. Phys. F*, **3**, 471-496.

EHRHARD, P. & SCHILLING, W. (1974). *Phys. Rev. B*, **8**, 2604-2621.

IIDA, A. (1979). *Phys. Status Solidi A*, **54**, 701-706.

IIDA, A. & KOHRA, K. (1979). *Phys. Status Solidi A*, **51**, 533-542.

LAL, K. (1981). *Proc. Indian Nat. Sci. Acad. Part A*, **47**, 20-46.

LARSON, B. C. (1975). *J. Appl. Cryst.* **5**, 150-160.

LARSON, B. C. & BARHORST, J. F. (1981). *Defects in Semiconductors*, pp. 151-162. Amsterdam: North-Holland.

LARSON, B. C. & SCHMATZ, W. (1974). *Phys. Rev. B*, **10**, 2307-2314.

LARSON, B. C. & YOUNG, F. W. JR (1973). *Z. Naturforsch. Teil A*, **28**, 626-632.

LOHSTÖTER, H., SPALT, H. & PEISEL, H. (1972). *Phys. Rev. Lett.* **29**, 224-226.

MAYER, W. & PEISEL, H. (1982). *J. Nucl. Mater.* **108 & 109**, 627-634.

PATEL, J. R. (1975). *J. Appl. Cryst.* **8**, 186-191.

RICHTER, H., MAI, M., KIRSCHT, F. G. & GAWORZEWSKI, P. (1983). *Physica (Utrecht)*, **116B**, 162.

SPALT, H. (1970). *Z. Angew. Phys.* **29**, 269-276.

THOMAS, J. E., BALDWIN, T. O. & DEDERICHS, P. H. (1971). *Phys. Rev. B*, **3**, 1167-1173.

ZAUMSEIL, P. & WINTER, U. (1982*a*). *Phys. Status Solidi A*, **70**, 471-496.

ZAUMSEIL, P. & WINTER, U. (1982*b*). *Phys. Status Solidi A*, **73**, 455-466.

Acta Cryst. (1985). A**41**, 227-232

Three-Crystal Diffractometry in Grazing Bragg–Laue Geometry

BY A. M. AFANAS'EV,* P. A. ALEKSANDROV,* R. M. IMAMOV, A. A. LOMOV & A. A. ZAVYALOVA

Institute of Crystallography of the USSR Academy of Sciences, Leninsky prospect 59, *Moscow* 117333, *USSR*

(*Received* 28 *March* 1984; *accepted* 19 *November* 1984)

Abstract

Three-crystal X-ray diffractometry (TCD) in grazing Bragg–Laue geometry has been experimentally realized for the first time. Theoretical simulations for the angular position and intensity of the main peak and the pseudopeak on TCD spectra have been obtained. It was established that TCD in grazing Bragg–Laue geometry has the following peculiarities: (1) the angular position and intensity of the main peak on the spectra depend on the sign of the deviation angle; (2) the main peak vanishes completely at negative deviation angles reaching the critical value; (3) the intensity of the main peak in grazing Bragg–Laue geometry is increased approximately by a factor of 10^2 (compared to symmetrical Bragg diffraction geometry). The above peculiarities were predicted theoretically and confirmed by experimental studies on ideal Si crystals.

Introduction

The method of three-crystal diffractometry (TCD) for the analysis of the angular distribution of diffracted X-rays (Eisenberger, Alexandropoulos & Platzman, 1972; Larson & Schmatz, 1974, 1980; Haubold & Martinsen, 1978; Iida & Kohra, 1979; Iida, 1979; Afanas'ev, Koval'chuk, Lobanovich, Imamov, Aleksandrov & Melkonyan, 1981; Zaumseil & Winter, 1982) is an effective method for investigating distortions in a crystal, in particular in its subsurface layers. TCD was traditionally used to measure diffuse scattering due to the defects of the crystal lattice (Larson & Schmatz, 1974, 1980; Ehrhart, 1978; Haubold & Martinsen, 1978; Iida & Kohra, 1979; Iida, 1979; Zaumseil & Winter, 1982). Recently some authors (Afanas'ev, Koval'chuk, Lobanovich, Imamov,

* Kurchatov Institute of Atomic Energy, Kurchatov square 46, Moscow 123182, USSR.

0108-7673/85/030227-06$01.50 © 1985 International Union of Crystallography